*Communications of the Geological Survey of Namibia, **29** (2026), 72-89*

Phengite formation at the contact between carbonatites and muscovite-kyanite schists: Kwaggaspan, northwestern Namibia

Roxanne Steffann[1,2], Benjamin F. Walter[2*], R. Johannes Giebel[3,4], Michael A. W. Marks[2], Andreja Ladisic[2], Lorenz Kemmler[2], Nicolas Schlosser[2], Thomas Binder[2], Felix Reinhard[2], Lukas Mössinger[2], Pascal Löschner[2], Saskia Dück[3] and Gregor Markl[2]

[1] University of Poitiers, Geoscience Department, 6 Rue Michel Brunet - Bât B35, 86073 Poitiers, France
[2] University of Tübingen, Petrology and Mineral Resources, Schnarrenbergstrasse 94-96, 72076 Tübingen, Germany
[3] Technische Universität Berlin, Angewandte Geochemie, Ernst Reuter Platz 1, 10587 Berlin, Germany
[4] University of the Free State, Department of Geology, 250 Nelson-Mandela-Drive, Bloemfontein 9300, South Africa

**Corresponding author: <b.walter@uni-tuebingen.de>*

Abstract :- This study investigates the previously unexamined Kwaggaspan Carbonatite Complex in northwestern Namibia, which intruded into muscovite-kyanite schist and quartzite of the Neoproterozoic Damara Supergroup, providing an ideal natural laboratory for examining the interaction between carbonatitic melts and SiO_2- and Al_2O_3-rich country rocks. A multi-analytical approach is employed, integrating petrographic analysis of thin sections, cathodoluminescence (CL) imaging, micro-X-ray fluorescence (µXRF) mapping, and electron microprobe analysis (EMPA).

Field and petrographic observations reveal that the Kuiseb Formation host schist has been metasomatically altered to quartz-phengite-magnetite rock during interaction with carbothermal brines. The formation of phengite highlights the so far undocumented interaction between a carbonatite melt and carbothermal brine, and a particularly Al-rich country rock. Chemical analyses of three distinct mica generations (F-bearing hydroxy-phlogopite, Fluoro-phlogopit and F-bearing phengite) record progressive alteration, driven by the influx of Al and Si from the surrounding country rock. The carbonatites display a well-defined crystallisation sequence, beginning with two generations of Fe-rich dolomite, followed by two generations of calcite. Metasomatic overprinting of the host rocks produced secondary mineral assemblages with baryte, monazite, pyrite, celestine, strontianite, and clinochlore. Supergene processes during later stages of alteration led to the pervasive development of Fe-oxides and natrojarosite throughout the system.

Keywords :- Carbonatite – country rock interaction, Muscovite-kyanite schist, Phengite, Al-contamination, Brine melt

Introduction

Carbonatites are igneous rocks with >25 vol.% primary carbonates (Tappe *et al*., 2025) and represent the most silica-poor magmas known (Mitchell, 2005; Woolley and Kjarsgaard, 2008; Jones *et al*., 2013; Schmidt *et al*.; 2024; Tappe *et al*., 2025). With about 600 occurrences worldwide, carbonatites include extrusive, intrusive, and carbothermal varieties (Mitchell, 2005), and are classified as calcite-, dolomite-, ankerite- or siderite carbonatites, as well as rare nyerereite carbonatites (Yaxley *et al*., 2022; Schmidt *et al*., 2024).

Interactions between diverse silicate country rocks and carbonatite magmas, and the associated possible reactions and interactions driven by the compositional gradients between magma and host rock remain poorly understood (Vasyukova and Williams-Jones, 2022; Anenburg and Walters, 2024). However, during such processes new lithologies may form at the interface between carbonatitic magma and the host rock, generating a progressive reaction front that affects both the country rock (via metasomatic replacement) and the carbonatite magma (Anenburg and Walters, 2024; Giebel *et al*., 2019; Gudelius *et al*., 2023; Vasyukova and Williams-Jones, 2022; Walter *et al*., 2023).

During differentiation and interaction, carbonatitic magma can gradually evolve towards a carbothermal or brine melt stage,

characterised by transitional fluid phases exhibiting properties intermediate between aqueous saline fluids and carbonate melts (e. g. Mitchell and Gittins, 2022; Anenburg and Walters, 2024). These solvent-rich fluids can mobilise high-field-strength (HFSE) and large-ion lithophile elements (LILE), including rare-earth elements (REE), Nb, Zr, Ti, Ta, U and Th. Such fluids are frequently associated with magmatic differentiation processes involving liquid immiscibility and exsolution, leading to separation of discrete melt and fluid phases (Walter *et al*., 2020, 2021; Ladisic *et al*., 2025; Raza *et al*., 2025).

The Kwaggaspan Carbonatite Complex in northwestern Namibia, which intruded into the Neoproterozoic Kuiseb schist (muscovite-kyanite schist; Fig. 1), presents a unique opportunity to investigate carbonatitic melt – country rock interaction processes, owing to the specific characteristics of both the host lithologies and the melts. Such metasedimentary rocks provide a valuable natural laboratory for constraining the physico-chemical reactions that may occur when high-temperature carbonatitic melts infiltrate and interact with metapelitic or quartz-rich protoliths (Walter *et al*., 2022, 2023), which is the scope of this contribution. In this context, as detailed below, the host rocks are identified as metapelites and metasandstones notably rich in Al_2O_3 and SiO_2, which exhibit extremely low solubility in carbonatitic melts (Vasyukova and Williams-Jones, 2022; Anenburg and Guzmics, 2023). Emphasis is placed on delineating the processes at the carbonatite – muscovite-kyanite schist/quartzite interface.

Geological setting

The Kwaggaspan Carbonatite Complex is situated some 55 km southeast of the town of Khorixas in the Erongo Region (northwestern Namibia; Fig. 1), which hosts several alkaline and carbonatitic complexes (Harris, 1995; Miller, 2008; Sun *et al*., 2024; Ladisic *et al*., 2025 and references therein). It forms intrusive plugs and dykes within the Neoproterozoic Kuiseb schist (Miller, 2008), which experienced greenschist facies metamorphism and has an estimated stratigraphic thickness of around ten kilometres. The formation is predominantly composed of muscovite-kyanite schist, with intercalated layers of quartzite and dolomite marble. The muscovite-kyanite schist is dominated by quartz, followed by alkali feldspar and muscovite, commonly accompanied by chlorite, kyanite and biotite (Miller, 2008). Deformation and faulting occurred in Pan-African time (535±13 Ma; Goscombe *et al*., 2003).

The five plugs comprising the Kwaggaspan Complex are aligned along a large-scale fold axis; two of them are rich in quartz, hematite, and muscovite, a further two are composed of fine-grained quartz and Fe-rich oxides and the remaining one is a coarse-grained dolomite-calcite carbonatite (Miller, 2008). The latter shows a well-defined outline and has a diameter of about 140 m. The other plugs, however, display a range of carbonatite-wall rock interaction zones, causing transgressive contacts with the country rocks. Coordinates of each sampling location are provided in Table 1.

Sample Name	Latitude (°)	Longitude (°)	Elevation (metres above sea level)
KWG001	-20.780866	15.272881	932
KWG002	-20.781063	15.273947	933
KWG003	-20.785562	15.278503	920
KWG004	-20.785574	15.278862	923

Table 1. Locations of the investigated samples

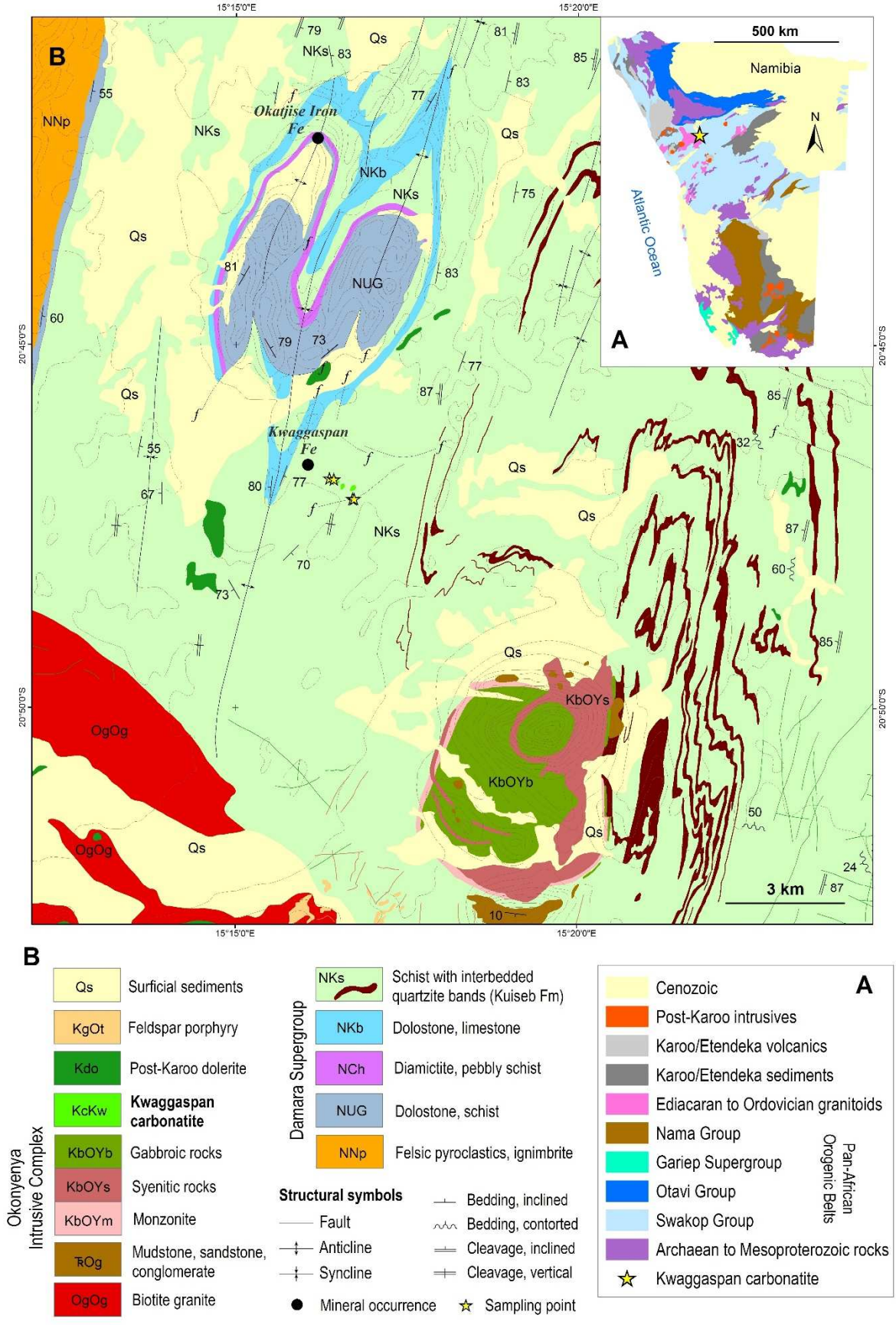

Figure 1. A) Simplified geological map of Namibia after Walter *et al*. (2023); B) Regional geological map showing the location of the Kwaggaspan carbonatites (modified after Geological Survey of Namibia, 2006)

Analytical methods

Thin sections of eleven representative samples from four locations were examined by transmitted and reflected light microscopy. Cathodoluminescence (CL) microscopy using a *Lumic HC6-LM* was performed with a vacuum pressure of 1 Pa, an accelerating voltage of 14 kV and a current of 0.4 mA. Scanning electron microscopy (SEM) was conducted with a *Phenom Tabletop SEM* in low vacuum mode (15 Pa), operating at 15 kV and 10 nA, with a working distance of 7 mm. Three selected polished specimens were analysed using a Bruker *Tornado Micro-X-Ray* system, and run with 50 kV accelerating voltage, 600 nA current, 20 µm beam diameter and 15 or 20 ms exposure time per pixel.

In addition, four thin sections were chosen for mineral chemistry analysis by electron microprobe (EMPA). Two are pure carbonatites and two represent the contact between host rock and carbonatite. The compositional data for micas and carbonates were obtained from an electron probe microanalyser JEOL JXA-8230, using albite (Na and Al), diopside (Mg and Si), sanidine (K), Cr metal (Cr), bustamite (Mn), $SrTiO_3$ (Sr and Ti), hematite (Fe), cryolite (F), tugtupite (Cl), LREE glasses (La, Ce, Pr and Nd), baryte (Ba) and calcite (C and Ca) as standards. Carbon was measured for matrix effects; however, due to carbon coating the content was calculated based on stoichiometric values. An acceleration voltage of 15 kV, a beam current of 20 nA and an electron beam diameter of 10 µm was used. The internal φ(ρz) correction was applied for data reduction. Peak counting times were 16 s for major elements and 30 s for minor elements, with background counting times being half that of peak times. Further details are given in Tables 2 and 3.

Element	Crystal	X-ray emission line	Standard	Peak counting time (s)	Average detection limit (ppm)
Na	TAPL	K_α	Albite	16	200
K	PTEJ	K_α	Sanidine	16	300
Mg	TAP	K_α	Diopside	16	250
Si	TAP	K_α	Diopside	30	250
Sr	PETL	L_α	$SrTiO_3$	16	500
Ba	LIFL	L_α	Baryte	30	700
La	LIFL	L_α	REE	30	850
Pr	LIFL	L_α	REE	30	900
Nd	LIFL	L_α	REE	30	700
Ca	PETJ	K_α	Calcite	16	400
Mn	PETJ	K_α	Bustamite	16	550
Fe	LIF	K_α	Hematite	16	500
Ce	LIF	L_α	REE	30	1400
C	LDE6H	K_α	Calcite	16	700

Table 2. EMPA programme parameters for carbonates

Element	Crystal	X-ray emission line	Standard	Peak counting time (s)	Average detection limit (ppm)
F	LDE1L	K_α	Cryolite	30	250
K	PTEJ	K_α	Sanidine	16	300
Mg	TAP	K_α	Diopside	16	250
Si	TAP	K_α	Diopside	16	200
Al	TAPL	K_α	Albite	16	150
Ba	PETL	L_α	Baryte	30	400
Na	TAP	K_α	Albite	30	200
Ti	PETL	K_α	$SrTiO_3$	30	200
Ca	PETL	K_α	Diopside	16	200
Mn	PETJ	K_α	Bustamite	30	450
Fe	LIF	K_α	Hematite	16	550
Cr	LIF	L_α	Cr	30	400
Cl	PETL	K_α	Tugtupite	30	75

Table 3. EPMA programme parameters for micas

Results

Petrography

A summary of the mineralogical composition of the investigated samples covering carbonatites and variably overprinted country rocks is provided in Table 4. The typical pelitic Kuiseb schist (sample KWG001B3; Figs 2a, b) mainly consists of micas, primarily muscovite I (and minor phlogopite) along with kyanite. The presence of both muscovite and kyanite underscores the high Al and Si content of the Kwaggaspan carbonatite host rocks. A holistic description of the Kuiseb schist is provided by Miller (2008).

SAMPLE										
KWG003B	KWG004A	KWG001B9	KWG001A1	KWG001A2	KWG001B4	KWG001A	KWG001B3	KWG001B1	KWG003A1	KWG003A2
LITHOLOGY										
carbonatite		carbonatite hosted basement xenolith	contact zone	overprinted country rock (muscovite kyanite schist)						
MINERALOGY										
mag, phl, dol, cal, hem/goe	mag, phl, dol, cal, clc/chl, py, mnz	Kfs, qtz, mag, Fphl-bt, cal, brt, hem/goe	Kfs, qtz, mag, phen, dol, cal, brt, hem/goe	Kfs, qtz, ms, mag, brt	qtz, ms, mag, brt, hem/goe	qtz, ms, mag, cal, brt, hem/goe	Kfs, zrn, qtz, ms, mag, cal, kya hem/goe	qtz, ms, mag, brt, clt, str, mnz, hem/goe	qtz, ms, mag, mnz, njrs, hem/goe	qtz, ms, mag, njrs

Table 4. Modal mineralogy of each sample: a quantification of celestine and strontianite was not possible in all samples. Mineral abbreviations based on Warr (2021): brt – baryte, cal – calcite, clc – clinochlore, clt – celestine, dol – dolomite, hem – hematite, Kfs – K-feldspar, kya – kyanite, mnz – monazite, ms – muscovite, mt – magnetite, njrs – natrojarosite, phl – phlogopite, py – pyrite, qz – quartz, phen – phengite, str – strontianite, zrn – zircon.

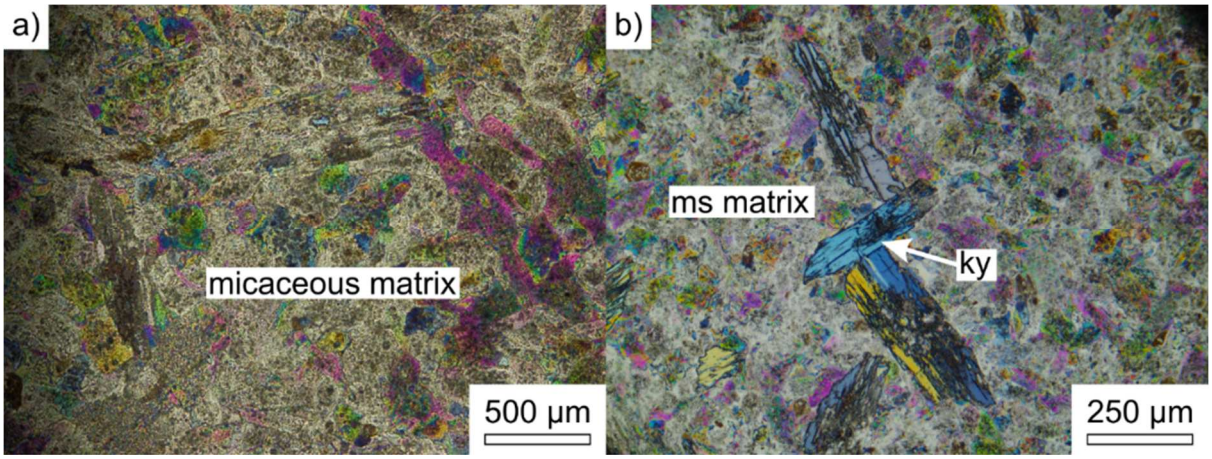

Figure 2. Thin section of sample KWG001B3 under polarised light: a) micaceous matrix with oriented kyanite relics; b) oriented kyanite phenocrysts aligned along foliation within a matrix of muscovite

Carbonatite

Carbonatites (samples KWG003B and KWG004) are composed predominantly of dolomite, which appears as two distinct generations (Fig. 3a, b). The first generation (dolomite I) is anhedral and partly altered to Fe-oxides (often along cleavages). The second generation (dolomite II) overgrows the earlier one, is euhedral and occurs adjacent to minor calcite, which is altered to a dark-brown to black halo of Fe-oxides. Similarly, two generations of calcite (I and II) are observed. Calcite I forms elongated crystals with well-defined chemical zoning, while calcite II is less abundant, finer-grained, and typically lacks the well-defined zoning observed in calcite I (Fig. 3c). Phlogopite occurs frequently and forms platy aggregates. Apatite is small in grain size and very rare. Also, magnetite is scarce in the carbonatites.

Contact zone between carbonatite and country rocks

Very close to the country rock (within a zone of 1-8 cm), xenocrysts of feldspar and quartz are entrained in the carbonatite (e. g. sample KWG001B9; Fig. 3d). In these contact zones, dolomite is typically absent, and calcite is the dominant carbonate together with variable amounts of quartz, altered K-feldspar (in xenoliths and overprinted country rocks), magnetite, phlogopite, and late-stage baryte and hematite. A typical contact zone between carbonatite and country rock (sample KWG001B9) is displayed in Figure 3d, showing the distribution of coarse and acicular calcite I (Sr-rich; Fig. 6c), finer-grained Mn-bearing calcite II, minor dolomite (Mg-rich areas in Fig. 6b), magnetite (Fe-rich areas), and baryte (S-rich areas), which are concentrated close to the contact with the country rock.

Some contact zones show a finer holocrystalline texture and significant alteration (e. g. KWG001A1), with extensive Fe-oxide coatings around minor calcite (Figs 3a, b). Here, the mineralogy is dominated by quartz, remnants of K-feldspar, calcite, baryte, magnetite, and abundant phengite (Figs 3e, f). The latter occasionally displays signs of mechanical stress (Fig. 3e).

Overprinted country rocks

In a decimetres to metres wide zone adjacent to the contact with the carbonatites, the muscovite-kyanite schists (e. g. sample KWG001B5) transition to a fine- to medium-grained magnetite-rich quartzite (Figs 3d, 4b). Two average grain sizes of quartz occur (Figs 4a, c). i. e. ~200 µm and ~50 µm. Cathodoluminescence (blue to red) reveals that both types exhibit polygonal grain contacts; some grains display growth zoning and striations, and luminescence locally changes from blue to orange-brown. Magnetite is abundant (30-250 µm), partly displaying pseudomorphic replacement after hematite or specularite. The samples contain numerous secondary minerals, dominated by baryte, which occurs as two generations: (1) euhedral phenocrysts up to 350 µm, and (2) anhedral pore-filling crystals. Other secondary minerals include pyrite, clinochlore, zircon (only in sample KWG001B-3; Fig. 4f), monazite, strontianite, celestine and

natrojarosite (Fig. 4d). The latter is an accessory mineral in sample KWG003A1, but a major phase (with quartz) in KWG003A2. Some country rock samples contain calcite veins (Fig. 4c) with a minor amount of dolomite. At the immediate contact of carbonatite with country rock, K-feldspar is recrystallised to muscovite II (Fig. 7). The complete paragenetic sequence is depicted in Figure 5.

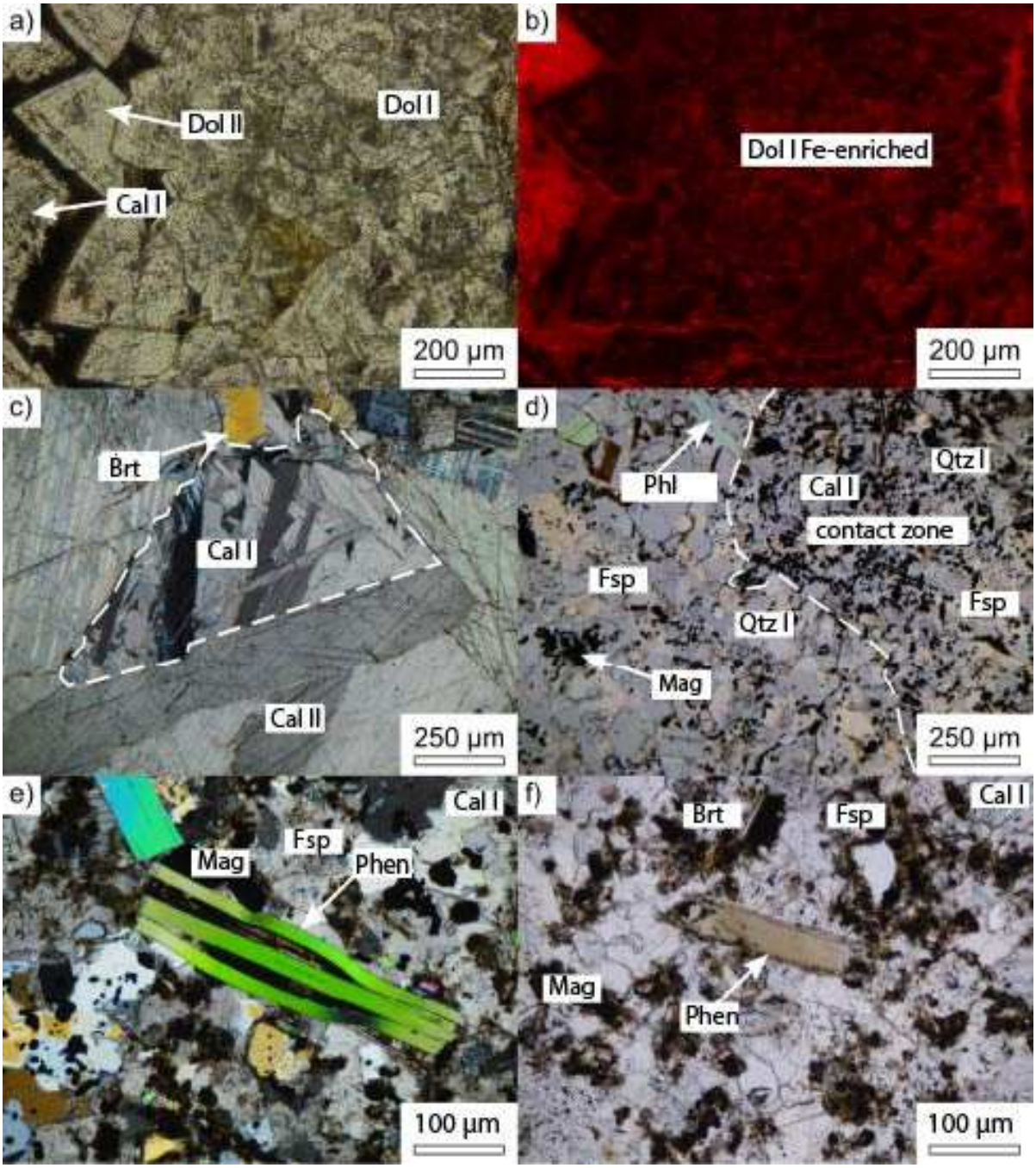

Figure 3. a) KWG003B in PPL (Plane-Polarised Light), two generations of dolomite: The first generation is anhedral and altered, while the second is euhedral and unaltered. An Fe-oxide halo formed around the calcite; b) KWG003B CL: both generations of dolomite are very rich in Fe, causing them to appear almost completely black; c) KWG001B-9 in XPL (Cross-Polarised Light): two generations of calcite differing in size and shape; d) KWG001B-9 in XPL: contact zone between the former carbonatitic melt and the wall rock (left); e) KWG001A-1 in XPL: mechanical stress causes the phengite to split along cleavages. However, no evidence of chemical alteration is observed; f) KWG001A-1 in PPL: phengite has undergone chemical alteration, as shown by a dissolution halo surrounding the grain.

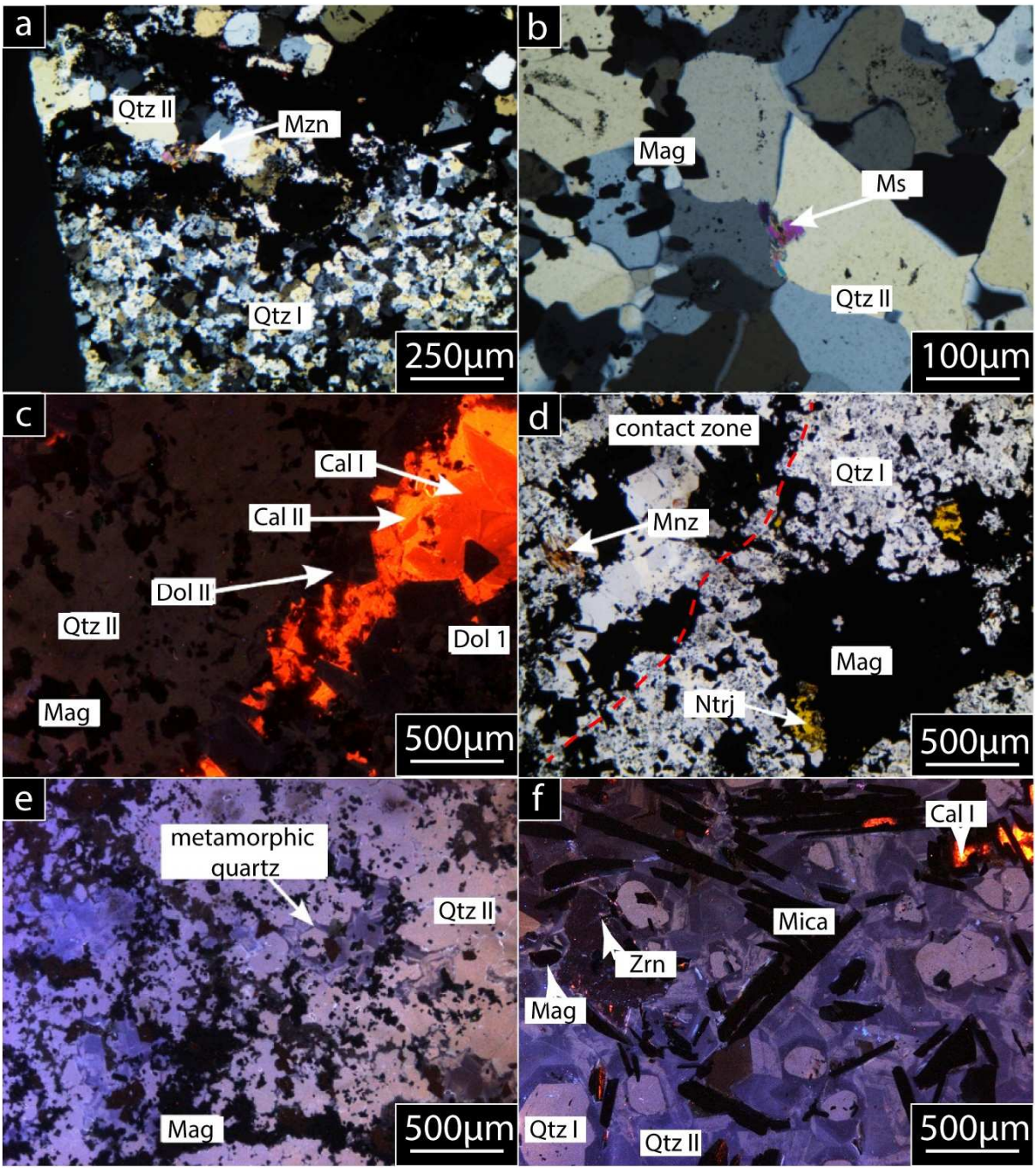

Figure 4. a) KWG001B4 in PPL: two generations of quartz are separated by magnetite. Aggregates of monazite are observed adjacent to magnetite and quartz; b) KWG001B4 in PPL: relicts of muscovite are found between the quartz grains; c) KWG001A CL: two calcite types are observed within the carbonatite vein. The calcite is separated from quartz by dolomite II. Dolomite I is present in much smaller amounts; d) KWG003A1 in PPL: natrojarosite associated with magnetite in altered quartz and accessory monazite; e) KWG001A6 CL: metamorphic and carbothermal quartz; f) KWG001B-3 CL: accessory zircon from the wall rock

Mineral compositions

Carbonates

Carbonates were analysed in carbonatites, contact zones and overprinted country rocks (samples KWG003B, KWG004A, KWG001B9, KWG001A1), with representative analyses given in Table 5. The two texturally distinguished dolomite generations (Figs 3a, 4c) show no discernable compositional differences, with FeO up to 4.7 wt% and MnO up to 0.45 wt%, although Fe increases

slightly with evolution (arrow in Fig. 8). Calcite I shows MnO up to 0.2 wt.%, whereas calcite II contains FeO <0.3 wt.% and MnO <2.7 wt.%, also with a slight increase as evolution progresses (arrow in Fig. 8).

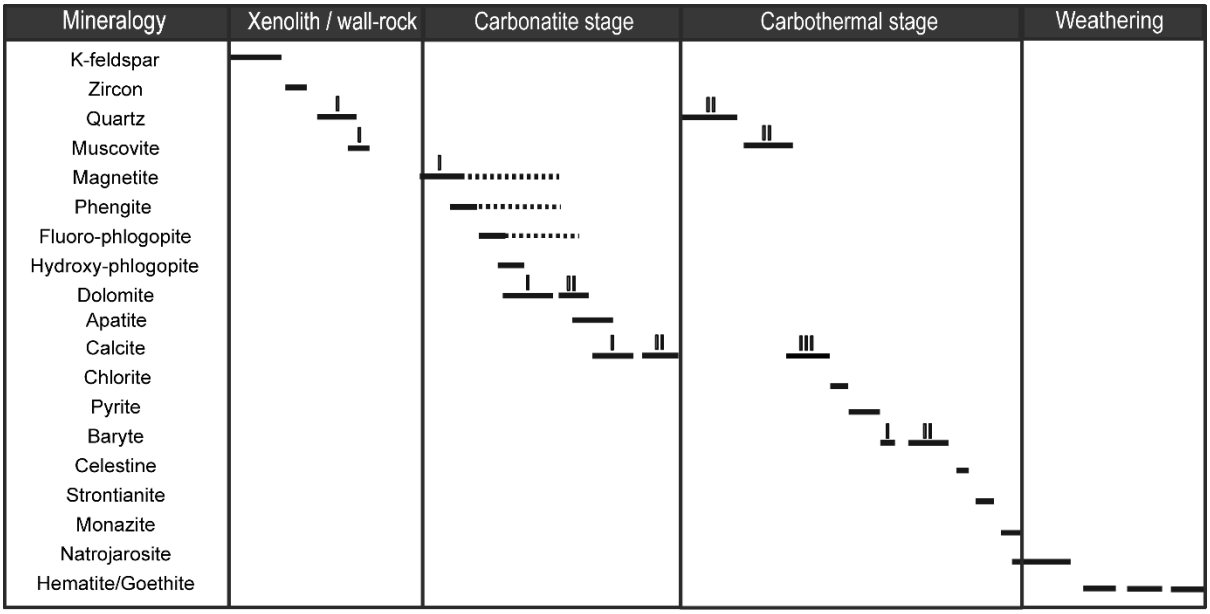

Figure 5. Paragenetic sequence: arrows represent the transformation of one mineral into another

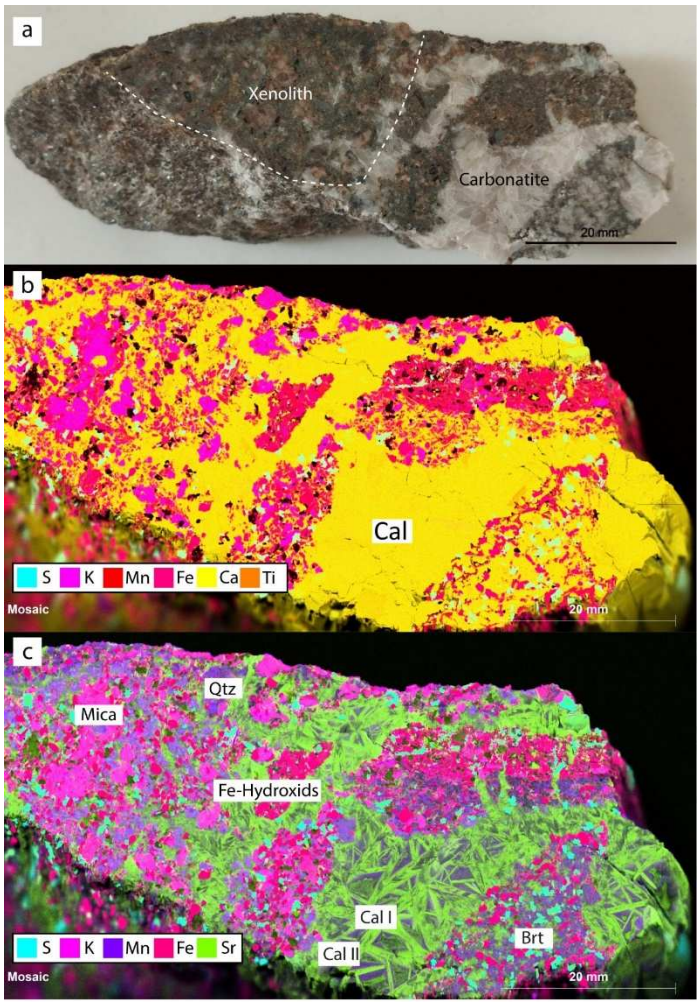

Figure 6. Various chemical maps obtained by µXRF on the polished section of sample KWG001B9 using the Mosaic option and element normalisation: a) Macroscopic photograph of the sample showing two distinct lithological domains: the dark one represents the wall rock and the light one corresponds to the carbonatite; b) elemental distribution map showing Mg, S, K, Ca, Ti, and Fe; c) Elemental distribution map showing S, K, Mn, Fe, and Sr

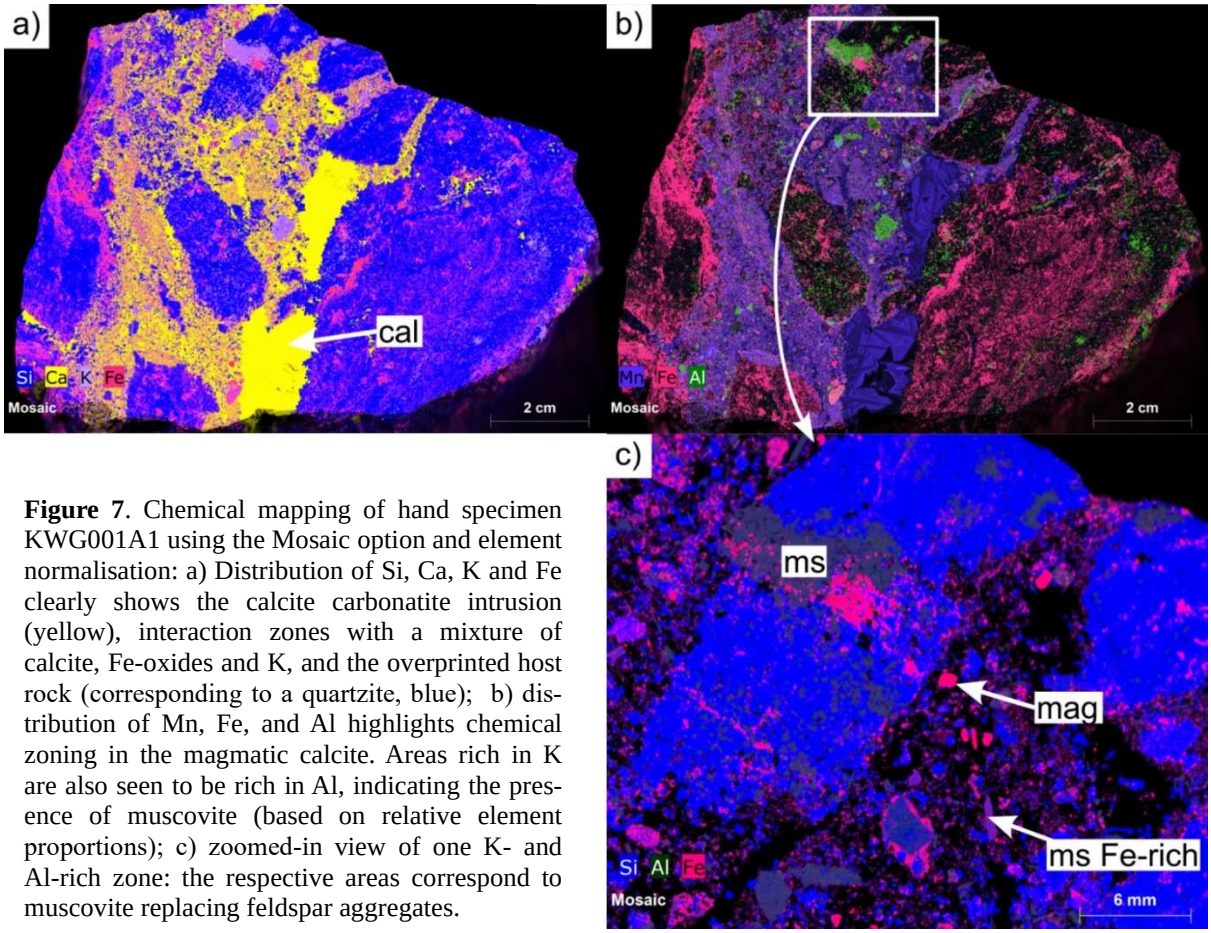

Figure 7. Chemical mapping of hand specimen KWG001A1 using the Mosaic option and element normalisation: a) Distribution of Si, Ca, K and Fe clearly shows the calcite carbonatite intrusion (yellow), interaction zones with a mixture of calcite, Fe-oxides and K, and the overprinted host rock (corresponding to a quartzite, blue); b) distribution of Mn, Fe, and Al highlights chemical zoning in the magmatic calcite. Areas rich in K are also seen to be rich in Al, indicating the presence of muscovite (based on relative element proportions); c) zoomed-in view of one K- and Al-rich zone: the respective areas correspond to muscovite replacing feldspar aggregates.

MINERAL	Fe-bearing dolomite	Ferroan dolomite	Calcite II	Fe-bearing calcite	Calcite II	Calcite I
FeO	2.5	4.66	0.2	0.27	b.d.l.	0.05
MnO	0.33	0.45	0.68	1.55	0.3	0.33
MgO	19.9	18.38	0.1	0.3	0.04	0.04
CaO	29.76	29.11	55.09	55.49	56.07	55.48
SrO	b.d.l.	b.d.l.	0.14	0.07	0.28	0.18
CO_2 calculated	46.88	46.09	43.97	45.06	44.39	43.96
Total	**99.53**	**98.81**	**100.26**	**102.79**	**101.17**	**100.17**
End member proportions						
$CaCO_3$	49.9	49.6	98.5	96.8	99.5	99.4
$MgCO_3$	46.4	43.6	0.2	0.7	0.1	0.1
$(Fe,Mn)CO_3$	3.7	6.8	1.2	2.5	0.4	0.5
Mineral formula						
Ca	0.5	0.5	0.98	0.97	0.99	0.99
Mg	0.46	0.43	>0.01	>0.01	>0.01	>0.01
Mn+Fe	0.04	0.07	0.01	0.03	>0.01	>0.01

Table 5. Exemplary mineral chemistry of carbonates: all analysed chemical elements are listed in their oxide forms, but for the calculation of the structural formula only Ca, Mg, Fe, and Mn were considered. Ba, Na, K, La, Ce, P, and Nd were in all samples below the detection limit and therefore omitted in the table.

Mica

Mica compositions were studied in three samples (KWG003B, KWG001B9 and KWG001A1; Table 6 & Fig. 9), and show distinct differences. Carbonatite (KWG003B) typically contains relatively pure phlogopite, low in both FeO (<2 wt.%) and F (<1.5 wt.%). Closer to the contact with the country rock (sample KWG001B9), phlogopite is higher in FeO (up to 4.6 wt.%) and F (up to 8.8 wt.%), while directly at the contact, within the country rock (KWG001A1), mica occurs as phengite with similar FeO (up to 4.5 wt.%) and F contents (up to 4.3 wt.%), but much higher Al_2O_3 (up to 26.6 wt.%).

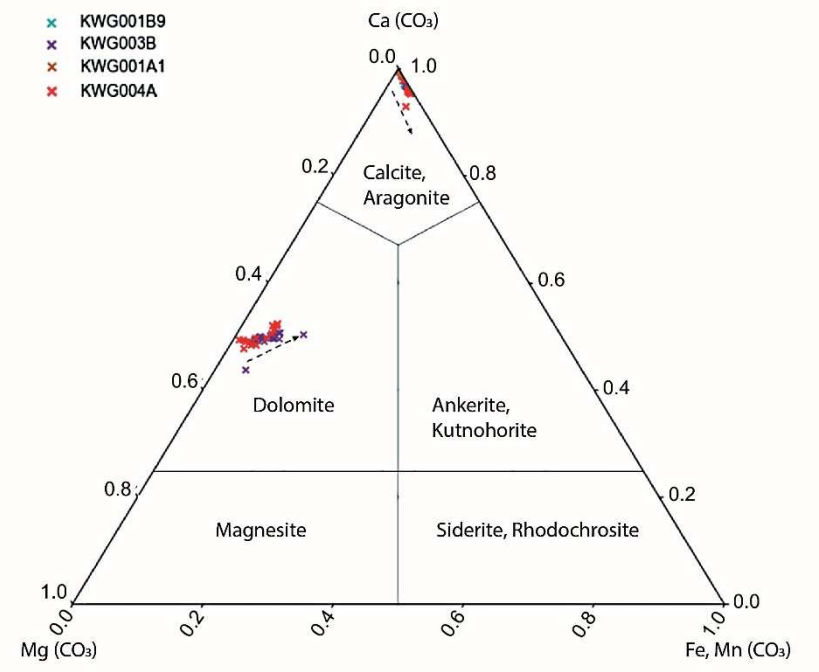

Figure 8. Ternary diagram showing the composition of carbonate; arrows indicate the evolutionary trajectory.

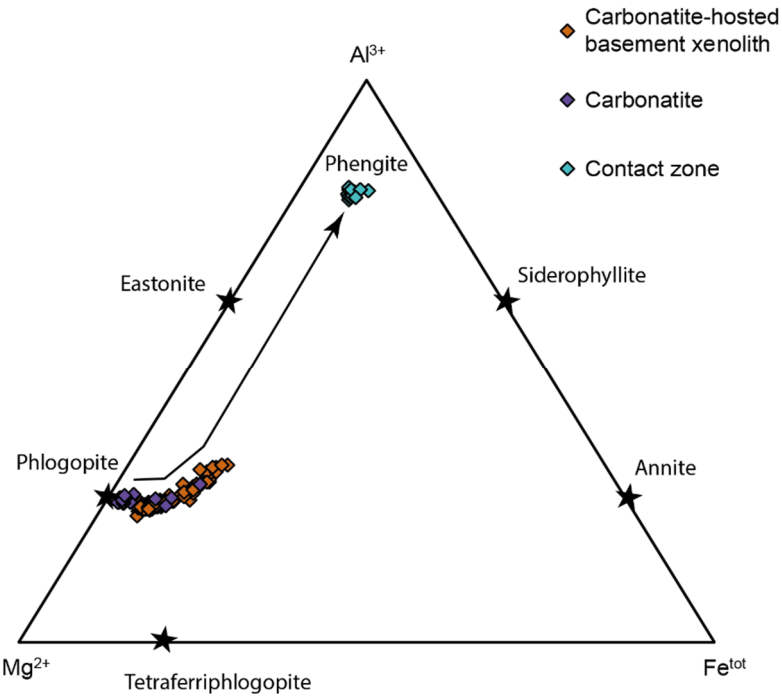

Figure 9. Ternary diagram of the mica mineral chemistry.

SAMPLE	KWG003B		KWG001B9	KWG001A1	KWG001A1	
LITHOLOGY	carbonatite		carbonatite hosted basement xenolith	contact zone	contact zone	
MINERAL	F-bearing hydroxy-phlogopite	F-bearing hydroxy-phlogopite	Fluoro-phlogopite	Fluoro-phlogopite	F-rich phengite	F-rich phengite
SiO_2	43.61	43.58	42.61	41.82	49.57	48.75
TiO_2	0.54	0.45	0.11	0.04	0.32	0.16
Al_2O_3	12.22	12.21	10.93	11.47	25.68	26.70
Fe_2O_3 (calc.)	0.00	0.00	0.06	0.07	0.00	0.00
FeO (calc.)	1.14	1.27	4.21	5.70	3.74	4.69
MgO	27.50	27.49	25.48	24.55	3.44	2.56
Na_2O	0.05	0.05	0.01	0.08	0.21	0.24
K_2O	10.59	10.59	10.85	10.77	11.35	11.22
F	2.53	2.42	8.45	8.29	3.85	3.33
Cl	0.07	0.09	0.03	0.10	0.01	0.01
H_2O (calc.)	2.53	2.63	0.00	0.15	2.59	2.82
$O=F_2,Cl_2$	1.08	1.04	3.56	3.51	1.62	1.4
Total	**99.7**	**99.7**	**99.2**	**99.5**	**99.1**	**99.1**
Si^{4+}	3.06	3.059	3.07	3.02	3.361	3.317
Ti^{4+}	0.028	0.024	0.006	0.002	0.017	0.008
Al^{3+}	1.011	1.01	0.927	0.976	2.052	2.141
Fe^{3+}	0.000	0.000	0.003	0.004	0.000	0.000
Fe^{2+}	0.067	0.075	0.254	0.348	0.211	0.266
Mg^{2+}	2.877	2.876	2.735	2.643	0.348	0.26
Ca^{2+}	0.000	0.000	0.000	0.000	0.000	0.000
Na^{+}	0.007	0.007	0.002	0.011	0.027	0.032
K^{+}	0.948	0.948	0.997	0.992	0.982	0.974
Total	**7.998**	**7.999**	**7.994**	**7.996**	**6.998**	**6.998**
F^{-}	0.561	0.537	1.925	1.893	0.826	0.717
Cl^{-}	0.009	0.011	0.003	0.012	0.001	0.002
OH^{-}	1.196	1.231	0.000	0.072	1.173	1.281
$O^{2-}=2-\Sigma(F,Cl,OH)$	0.234	0.221	0.072	0.023	0.000	0.000
Total	**2.000**	**2.000**	**2.000**	**2.000**	**2.000**	**2.000**

Table 6. Exemplary mineral chemistry of mica: Ca, Ba, Cr, and Mn were analysed, but are below the detection limit and therefore omitted in the table.

Discussion

Evolution of the Kwaggaspan Carbonatite Complex

The earliest carbonate phase to crystallise in the carbonatites from Kwaggaspan is ferroan dolomite. The crystals exhibit Fe exsolution at their margins, forming dark Fe-oxide rims that physically separate them from the later crystallised calcite (Figs 3a, b). This sequence represents an inversion of the expected carbonate crystallisation order (Gittins and Harmer, 1997; Woolley and Kjarsgaard, 2008; Mitchell, 2005; Jones *et al*., 2013; Tappe *et al*., 2025), with calcite forming only after the precipitation of ferroan dolomite.

Two non-exclusive hypotheses may explain the observed inversion despite the prima-

ry melt's Mg-enrichment. (i) Kinetic control by melt composition and redox conditions: primary carbonatitic melts are typically Mg-rich (Jones *et al*., 2013) and calcite crystallises first due to its higher thermodynamic stability (Schmidt *et al*., 2024). The addition of Fe can shift stability towards hypersolvus Mg/Fe-rich calcite and narrow the dolomite field (or towards Fe-rich carbonates such as ankerite; Schmidt *et al*., 2024). Experimental work shows that Fe/Mg-bearing melts reach dolomite saturation prior to calcite under specific P-T-X(CO_2) conditions (Richert and Schmidt, 2025). (ii) Secondary dissolution and replacement: initial crystallisation starts with calcite, but was followed by subsequent dissolution and replacement by dolomite, possibly through metasomatic processes or fluid-rock interaction during magmatic or post-magmatic stages. The latter has been documented in natural systems (e. g. Chakhmouradian *et al*., 2016; Vasyukova and Williams-Jones, 2022; Gudelius *et al*., 2023), and from sedimentary systems such a replacement is well known (e. g. Mueller *et al.,* 2020; 2022; 2024). Notably, in the investigated samples calcite is more abundant in the contact zones near the host rock, as has been observed also in the Eureka (Namibia) carbonatite (Adamcova, 2025).

Slight enrichment of Fe in dolomite and calcite, as observed in the present study (Fig. 8), is a common feature in evolving carbonatitic systems (Gittins and Harmer, 1997; Woolley and Kjarsgaard, 2008; Mitchell, 2005; Jones *et al*., 2013; Tappe *et al*., 2025). Two interpretations are considered for such a systematic variation. (i) Progressive Fe incorporation during crystallisation: during magmatic differentiation, Fe^{2+} may substitute for Ca^{2+} in calcite as the availability of Ca in the melt diminishes; (ii) post-crystallisation alteration: Fe originally incorporated in calcite could have been leached during later carbothermal alteration, resulting in Fe-depleted, relatively pure calcite. Based on Fe-enrichment along cleavages, post-crystallisation alteration is rather more likely than purely magmatic crystallisation, which would lead to growth zones. Chemical evolution of the different calcite generations observed by µXRF analysis (Fig. 6) provides insights into the crystallisation history of calcite carbonatite. Strontium is preferentially concentrated in the early, elongated calcite crystals, suggesting early and rapid crystallisation from a Sr-rich melt. In contrast, Mn is enriched in more peripheral growth zones, indicating slower crystallisation at a later stage. The partitioning behaviour of these elements is consistent with their ionic properties: Sr^{2+} readily substitutes for Ca^{2+} at elevated temperatures (550–700 °C), while Mn^{2+} incorporation into calcite is more favourable at lower temperatures (250–450 °C) or once Sr saturation is reached (Reeder, 1983). Such development is characteristic of differentiated carbonatites and may also indicate magmatic replenishment or remobilisation by late-stage fluids, potentially of carbothermal origin (involvement of aqueous fluids is indicated by the formation of chlorite and muscovite; Reeder, 1983).

Moreover, a carbothermal stage can be assumed for monazite, which occurs as fine-grained, acicular aggregates dispersed within the carbonatite, the contact zone and the overprinted country rock. Its small grain size and clustered texture are consistent with rapid crystallisation from a probably low-temperature fluid or a brine melt (Anenburg *et al*., 2021). The origin of this mineral is therefore more likely carbothermal than magmatic. The spatial association of monazite with baryte and strontianite also supports precipitation from a REE-enriched carbothermal residue, rather than direct magmatic crystallisation (Walter *et al*., 2022). Monazite formation therefore likely represents low-temperature fluid reaction with country rocks, as has also been described from the Eureka carbonatite in central Namibia (Broom-Fendley *et al*., 2020; Adamcova, 2025).

Mineralogical overprint in the country rock

The overprinted country rocks are predominantly Fe-rich quartzites, marked by the presence of multiple generations of feldspar, magnetite and other Fe-oxides; they also contain muscovite (replacing K-feldspar). The observed mineralogical complexity is interpreted as the result of extensive overprinting due to infiltration of the evolved carbonatite magma/carbothermal residues. Such processes are common in late-stage carbonatitic systems and often lead to the formation of a wide suite of secondary minerals, which will be discussed in the following.

Formation of baryte, strontianite, and natrojarosite

Baryte typically precipitates during the late magmatic to post-magmatic stages of carbonatite evolution (Walter *et al*., 2020, 2021). Upon migration into the surrounding wall rock, these evolved carbonatites/carbothermal residues may encounter chemically and physically distinct environments (often with contrasting pH, redox potential, or ionic activity) leading to baryte precipitation. Baryte is observed in association with pyrite, monazite, hematite and micas in the host rock, further supporting its carbothermal origin. A first generation of well-crystallised baryte likely precipitated under stable conditions at 150-300 °C (Reeder, 1983). A second generation of anhedral baryte fills pore spaces and suggests rapid precipitation from a late-stage or transient carbothermal event.

Under such conditions baryte may crystallise before or concurrently with celestine, provided the fluid is not too highly oxidising. In contrast, celestine forms from interaction between Sr-rich fluids and oxidising, sulfate-rich environments, often within carbothermal veins, or it occurs disseminated in altered carbonates. The required sulfate may originate from the oxidative dissolution of sulfide minerals such as pyrite. This low-temperature mineral assemblage further supports a low-temperature, post-magmatic carbothermal event affecting the country rock.

Most pyrite in the altered country rocks is replaced by natrojarosite, which indicates acidic fluid circulation following carbonatite emplacement under weathering conditions. It may form through either carbothermal alteration, where pyrite oxidation produces SO_4^{2-}-rich, acidic fluids that interact with Na-bearing silicates (mainly feldspars), or via supergene weathering, where oxidised meteoric waters react with sulfide-rich rocks, transforming pyrite into natrojarosite (Desborough *et al*., 2010). In either case, a sulfur-bearing precursor, most likely pyrite, is required. The isometric shapes and spatial distribution of natrojarosite within the rock support its derivation from pyrite. This transformation is common in weathering and hydrothermal systems and marks significant supergene alteration in the Kwaggaspan Complex.

Formation of phengite

The compositional variation of mica in carbonatites has been used to track magma evolution and magma - host rock interaction (e. g. Giebel *et al*., 2019). Typically, mica in carbonatites evolves from phlogopite to eastonite or tetraferriphlogopite and, in the case of wall rock interaction, phlogopite evolves into biotite and subsequently into annite (Giebel *et al*., 2019). In contrast, the present study reveals a distinctly different evolution trajectory from phlogopite to slightly aluminous Fe-rich phlogopite, culminating in the formation of phengite (Fig. 9), and characterised by increasing Fe and Al. This trend is attributed to interaction with the metapelitic, and exceptionally Al-rich country rock (Kuiseb schist), which is notably enriched in muscovite and kyanite (Fig. 2). The high Al-content of the host rock appears to have been a major factor influencing mica composition during interaction.

The mica crystallisation sequence is summarised in Figure 10. Initially, phengite forms within the contact zone during extensive melt – wall rock interaction. The interaction involves Si and Al from the metasedimentary host rock and Fe and F from the infiltrating carbonatitic melt. Subsequently, Fe-rich phlogopite crystallises within the contact zone, reflecting mixed chemical input: Si and Al from the host rock, and Fe, Mg and F from the intruding melt. In the final stage, phlogopite crystallises at lower temperatures, when much of the fluorine has already been incorporated into earlier micas (continuous consumption of fluorine during mica formation). This phase forms at the interface between the melt and host rock and, later, within the melt itself, explaining its restriction to carbonatitic domains.

Emplacement model and evolution of the carbonatitic system

The emplacement of the carbonatitic plugs remains a theoretical reconstruction, inferred primarily from the spatial distribution of sampling points (Figure 1). The curved alignment of these locations, combined with the presence of surrounding fault zones, suggests that the carbonatitic magmas ascended along a zone of structural weakness, possibly

the broken axis of a steeply dipping fault. It is proposed that the carbonatitic plugs ascended along this fault system. Since deformation in the area is dated to Pan-African time (535±13 Ma, Goscombe *et al*., 2003), a lower age-limit for the intrusion can be structurally defined. However, a Mesozoic age is more likely due to the adjacent Okenyenye grabbroic intrusion dated at 123.4±1.4 Ma (Milner *et al*., 1993). Nevertheless, Permian and Triassic ages are known from the carbonatites of the Damaraland Igneous Province (Sun *et al*., 2024; Ladisic *et al*., 2025) and therefore the Kwaggaspan Complex could also be part of an earlier carbonatite event. A more specific time frame of intrusion cannot be given at this time.

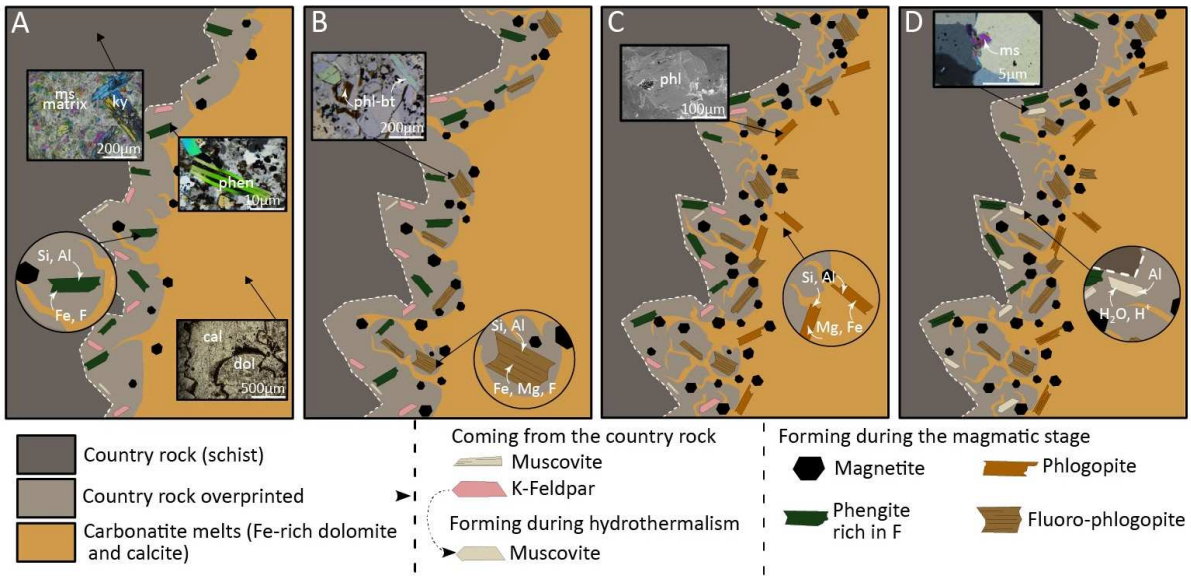

Figure 10. Conceptual diagram of mica evolution and crystallisation: A) Representation of the three different lithologies during the magmatic episode, showing the key minerals inherited from the country rock and the formation of phengite through interaction between the carbonatitic melt and the overprinted country rock; B) at a later magmatic stage, formation of fluoro-phlogopite through continued interaction between the carbonatitic melt and the overprinted country rock occurred close to the carbonatitic melt; C) formation of phlogopite at an even later magmatic stage through interactions between the carbonatitic melt and the overprinted country rock. Formed right at the interface, these minerals, along with part of the magnetite, precipitate directly from the carbonatitic melt; D) during carbothermal alteration, chemical reactions involving feldspar result in muscovite crystallisation.

Upon emplacement, the carbonatites interacted with the surrounding country rock, triggering metasomatic reactions that resulted in the observed mineralogical complexity described above. The strongly overprinted host rock is characterised by quartz, destabilised alkali feldspar, secondary mica and abundant magnetite, underlining the Fe-rich nature of the evolved carbonatites.

The magmatic sequence started with the crystallisation of Fe-rich dolomite, forming first anhedral, then euhedral crystals, with Mg progressively substituted by Fe. Calcite represents the final magmatic phase. Carbothermal activity appears to start during late magmatism, as indicated by the presence of baryte at the carbonatite – country rock interface, reflecting early fluid migration. Carbothermal alteration persists at 250–350 °C, causing quartz recrystallisation, polygonal grain boundaries, and abundant fluid inclusions. Clinochlore begins to crystallise in the carbonatitic units with continued cooling, and is followed by pyrite and two generations of baryte.

Late-stage fluids (200–300 °C) enable the formation of secondary calcite, pyrite, baryte, celestine, strontianite, and monazite. Iron-depleted calcite II forms through alteration of older carbonates. Supergene alteration produces natrojarosite from pyrite, and Fe-oxides (e. g. goethite, hematite) display diverse textures: (i) coarse crystals up to 200 µm; (ii) fine crystals <10 µm; and (iii) spheroidal coatings on pre-existing minerals (e. g. natrojarosite) forming a gossan.

Conclusions

The Kwaggaspan Carbonatite Complex forms several plugs and associated veins, which intruded the Kuiseb schist. Intense interaction between the evolved carbonatites and the host schist produced decimetre-thick, Fe-rich, quartzite-like rocks interpreted as strongly metasomatised country rocks, and led to the formation of phengite. Following this metasomatic overprint, the carbonatitic melt crystallised in a distinctive sequence: two generations of Fe-rich dolomite, succeeded by two generations of calcite. A subsequent carbothermal episode led to the formation of clinochlore, pyrite, baryte, strontianite, celestine, and monazite. Finally, ongoing supergene alteration, in conjunction with the system's Fe-rich character, produced abundant Fe-oxides, such as hematite and goethite. In the course of weathering-related processes, natrojarosite forms through the oxidative alteration of pyrite.

Acknowledgements

This study is supported by DFG (Deutsche Forschungsgemeinschaft) grants (WA 3116/3-1, WA 3116/9-1, WA 3116/28-1; MA 2563/21-1, MA 2135/26-1, GI 1499/11-1, GI 1499/5-1) to Benjamin Walter, Johannes Giebel, Gregor Markl and Michael Marks. Financial support is also provided to the first author by EUR INTREE, the University of Poitiers (France), and the Erasmus+ programme. Tim Langner, Martina Brenn and Simone Schafflick are thanked for their support during sample preparation. Christoph Glotzbach is thankfully acknowledged for trying age dating on the complex. Editors and reviewers are thanked for constructive criticism.

References

Adamcova, A. 2025. Antiskarn formation in the Eureka carbonatite. BSc thesis, Technical University of Berlin, 59 pp.

Anenburg, M., Broom-Fendley, S. and Chen, W. 2021. Formation of rare earth deposits in carbonatites. *Elements*, **17(5)**, 327-332.

Anenburg, M. and Guzmics, T. 2023. Silica is unlikely to be soluble in upper crustal carbonatite melts. *Nature Communications*, **14(1)**, https://www.nature.com/articles/s41467-023-35840-6

Anenburg, M. and Walters, J. B. 2024. Metasomatic ijolite, glimmerite, silicocarbonatite, and antiskarn formation: carbonatite and silicate phase equilibria in the system Na_2O–CaO–K_2O–FeO–MgO–Al_2O_3–SiO_2–H_2O–O_2–CO_2. *Contributions to Mineralogy and Petrology*, **179(5)**, https://doi.org/10.1007/ s00410-024-02109-0

Broom-Fendley, S., Smith, M. P., Andrade, M. B., Ray, S., Banks, D. A., Loye, E., Atencio, D., Pickles, J. R. and Wall, F. 2020. Sulfur-bearing monazite-(Ce) from the Eureka carbonatite, Namibia: oxidation state, substitution mechanism, and formation conditions. *Mineralogical Magazine*, **84(1)**, 35-48.

Chakhmouradian, A. R., Reguir, E. P. and Zaitsev, A. N. 2016. Calcite and dolomite in intrusive carbonatites. I. Textural variations. *Mineralogy and Petrology*, **110(2)**, 333-360.

Desborough, G. A., Smith, K. S., Lowers, H. A., Swayze, G. A., Hammarstrom, J. M., Diehl, S. F., Leinz, R., and Driscoll, R. L. 2010. Mineralogical and chemical characteristics of some natural jarosites. *Geochimica et Cosmochimica Acta*, **74(3)**, 1041-1056.

Geological Survey of Namibia. 2006. *Geological Map of Area 2014 Fransfontein*, 1:250 000 scale series. Ministry of Mines and Energy, Windhoek, Namibia.

Goscombe, B., Hand, M. and Gray, D. 2003. Structure of the Kaoko Belt, Namibia: progressive evolution of a classic transpressional orogen. *Journal of Structural Geology*, **25(7)**, 1049-1081.

Giebel, R. J., Parsapoor, A., Walter, B. F., Braunger, S., Marks, M. A., Wenzel, T. and Markl, G. 2019. Evidence for magma–wall rock interaction in carbonatites from the

Kaiserstuhl Volcanic Complex (Southwest Germany). *Journal of Petrology*, **60(6)**, 1163-1194.

Gittins, J. and Harmer, R.E. 1997. What is ferrocarbonatite? A revised classification. *Journal of African Earth Sciences*, **25(1)**, 159-168.

Gudelius, D., Marks, M.W., Markl, G., Nielsen, T.F., Kolb, J. and Walter, B. 2023. The origin of ultramafic complexes with melilitolites and carbonatites: a petrological comparison of the Gardiner (E Greenland) and Kovdor (Russia) intrusions. *Journal of Petrology*, **64(6)**, https://doi.org/ 10.1093/petrology/egad036

Harris, C. 1995. Oxygen isotope geochemistry of the Mesozoic anorogenic complexes of Damaraland, northwest Namibia: evidence for crustal contamination and its effect on silica saturation. *Contributions to Mineralogy and Petrology*, **122(3)**, 308-321.

Jones, A. P., Genge, M. and Carmody, L. 2013. Carbonate melts and carbonatites. *Reviews in Mineralogy and Geochemistry*, **75(1)**, 289-322.

Ladisic, A., Marks, M.A., Walter, B.F., Giebel, R.J., Beranoaguirre, A. and Markl, G., 2025. Permo-Triassic magmatism in the Damaraland Igneous Province, NW Namibia: The Ondurakorume alkaline-carbonatite complex. *Geochemistry*, **85(3)**, https://doi.org/10.1016/j.chemer.2025.126287

Miller R. McG. 2008. Neoproterozoic and early Palaeozoic rocks of the Damara Orogen. *In*: Miller, R. McG. (Ed.). *The Geology of Namibia*, Vol. **2**, chapter 13, 410 pp. Geological Society of Namibia, Windhoek.

Milner, S. C., Le Roex, A. P. and Watkins, R. T. 1993. Rb-Sr age determinations of rocks from the Okenyenya igneous complex, northwestern Namibia. *Geological Magazine*, **130(3)**, 335-343.

Mitchell, R. H. 2005. Carbonatites and carbonatites and carbonatites. *The Canadian Mineralogist*, **43(6)**, 2049-2068.

Mitchell, R. H. and Gittins, J. 2022. Carbonatites and carbothermalites: A revised classification. *Lithos*, **430-431**, https://doi.org/10.1016/j.lithos.2022.106861

Mueller, M., Igbokwe, O. A., Walter, B., Pederson, C. L., Riechelmann, S., Richter, D. K., Albert, R., Gerdes, A., Buhl, D., Neuser, r., Bertotti, G., and Immenhauser, A. 2020. Testing the preservation potential of early diagenetic dolomites as geochemical archives. *Sedimentology*, **67(2)**, 849-881.

Mueller, M., Jacquemyn, C., Walter, B. F., Pederson, C. L., Schurr, S. L., Igbokwe, O. A., Jöns, N.Richelmann, S., Dietzel, M., Strauss, H., and Immenhauser, A. 2022. Constraints on the preservation of proxy data in carbonate archives–lessons from a marine limestone to marble transect, Latemar, Italy. *Sedimentology*, **69(2)**, 423-460.

Mueller, M., Walter, B. F., Giebel, R. J., Beranoaguirre, A., Swart, P. K., Lu, C., Riechelmann, S., and Immenhauser, A. 2024. Towards a better understanding of the geochemical proxy record of complex carbonate archives. *Geochimica et Cosmochimica Acta*, **376**, 68-99.

Raza, M., Giebel, R. J., Staude, S., Beranoaguirre, A., Kolb, J., Markl, G. and Walter, B. F. 2025. The magmatic to post-magmatic evolution of the Nooitgedacht Carbonatite Complex, South Africa. *Geochemistry*, **85(1)**, https://doi.org/10.1016/j.chemer.2025.126249

Reeder, R. J. 1983. Crystal chemistry of the rhombohedral carbonates. *Reviews in Mineralogy and Geochemistry*, **11(1)**, 1-47.

Richert, P. M. and Schmidt, M. W. 2025. Crustal evolution of carbonatitic melts: Insights from the $CaCO_3$–$MgCO_3$–Na_2CO_3 ternary. Abstracts Goldschmidt 2025 Conference, *6-11 July*, Prague, Czech Republic, https://conf.goldschmidt.info/goldschmidt/2025/meetingapp.cgi/Paper/30031

Schmidt, M.W., Giuliani, A. and Poli, S. 2024. The origin of carbonatites—combining the rock record with available experimental constraints. *Journal of Petrology*, **65(10)**, https://doi.org/10.1093/petrology/egae105

Sun, Y., Galli, A., Szymanowski, D., Guillong, M., Rosskopf, R., Simon, J., Shipandeni, A. and Bachmann, O. 2024. High-precision zircon geochronology and geochemistry of evolved magmatic centres in the Paraná-Etendeka LIP: Temporal placement and tectono-magmatic origin of the Damaraland complexes, Namibia. *Lithos*, **480-481**, https://doi.org/10.1016/j.lithos.2024.107651

Tappe, S., Beard, C. D., Borst, A. M., Humphreys-Williams, E. R., Walter, B. F. and Yaxley, G. M. 2025. Kimberlite, carbonatite and alkaline magmatic systems: definitions,

origins, and strategic mineral resources. *EarthArXiv Preprints*, https://eartharxiv.org/repository/view/8658/

Vasyukova, O. V. and Williams-Jones, A. E. 2022. Carbonatite metasomatism, the key to unlocking the carbonatite-phoscorite-ultramafic rock paradox. *Chemical Geology*, **602**, https://doi.org/10.1016/j.chemgeo.2022.120888

Walter, B. F., Steele-MacInnis, M., Giebel, R. J., Marks, M. A. and Markl, G. 2020. Complex carbonate-sulfate brines in fluid inclusions from carbonatites: Estimating compositions in the system H2O-Na-K-CO3-SO4-Cl. *Geochimica et Cosmochimica Acta*, **277,** 224-242.

Walter, B. F., Giebel, R. J., Steele-MacInnis, M., Marks, M. A., Kolb, J. and Markl, G., 2021. Fluids associated with carbonatitic magmatism: A critical review and implications for carbonatite magma ascent. *Earth-Science Reviews*, **215**, https://doi.org/10.1016/j.earscirev.2021.103509

Walter, B. F., Giebel, J., Marlow, A. G., Siegfried, P. R., Marks, M., Markl, G., Palmer, M. and Kolb, J. 2022. The Keishöhe carbonatites of southwestern Namibia–the post-magmatic role of silicate xenoliths on REE mobilisation. *Communications of the Geological Survey of Namibia*, **25**, 1-31.

Walter, B. F., Giebel, R. J., Siegfried, P. R., Gudelius, D. and Kolb, J. 2023. The eruption interface between carbonatitic dykes and diatremes – The Gross Brukkaros volcanic field Namibia. *Chemical Geology*, **621**, https://doi.org/10.1016/j.chemgeo.2023.121344

Warr, L. N. 2021. IMA–CNMNC approved mineral symbols. *Mineralogical Magazine*, **85(3)**, 291-320.

Woolley, A. R. and Kjarsgaard, B. A. 2008. Paragenetic types of carbonatite as indicated by the diversity and relative abundances of associated silicate rocks: evidence from a global database. *The Canadian Mineralogist*, **46(4)**, 741-752.

Yaxley, G.M., Anenburg, M., Tappe, S., Decree, S. and Guzmics, T. 2022. Carbonatites: classification, sources, evolution, and emplacement. *Annual Review of Earth and Planetary Sciences*, **50(1)**, 261-293.